Original Article

Proc IMechE Part J:
J Engineering Tribology
2014, Vol. 228(8) 836–848

DOI: 10.1177/1350650114533101
pij.sagepub.com

Steady state and dynamic characteristics for guide bearings of a hydro-electric unit

Gregory F Simmons[1,2], Matthew Cha[3], Jan-Olov Aidanpää[4], Michel J Cervantes[5] and Sergei Glavatskih[3,6]

Abstract

Experiments are conducted using a 10-MW Kaplan hydropower machine which is outfitted with an extensive array of sensors to determine oil film thickness, pad load and oil temperature in all three guide bearings as well as motion of the shaft in relation to both the bearing housings and the concrete foundation. Test results for all journal bearings are compared to a commercial rotor dynamics model and results for the central journal bearing are compared to a multi-physics model to provide insight into the machine's steady state and dynamic characteristics and their variations during normal operation.

Keywords

Tilting pad, hydropower, journal bearing

Date received: 11 September 2013; accepted: 4 April 2014

Introduction

De-regulation of electricity markets and the build-up of intermittent power sources such as wind and solar have led to changes in the way that hydro-electric power plants operate. Traditionally, large hydro-power plants have provided steady power supply to the grid with machines operating at or near maximum efficiency with minimal adjustments and few starts and stops. However, because of ongoing changes in the electrical power network, hydro-electric machines are more often used to provide regulating power to maintain grid frequency. This leads to operation outside of ideal operating ranges as well as an increase in starts and stops which can lead to larger dynamic loads and increased wear and tear on the machine. Thus, a clear understanding of the machine's dynamic characteristics is essential for safe operation.

The dynamics of journal/guide bearings are generally well understood with a large body of work covering bearing design and modeling as well as experimental results. The body of this work is summarized by Dimond et al.[1] Nearly all of the work on journal bearings has focused on horizontal machines in which gravity provides a key stabilizing force.

On the contrary, most hydropower machines have vertical shafts with essentially no stabilizing load which results in potentially large shaft orbits and a greater sensitivity to other excitations. Study of a vertical rotor and machine by White et al.[2] found that dramatically decreasing the radial clearance in a pump's journal bearings moved a critical speed outside of the machine's operating range. Another study of vertical bearings by San Andres and De Santiago[3] found that the characteristics of a vertical plain bearing under high load could generally be predicted by modeling it as a horizontal configuration but that the fluid inertia terms were significantly greater in the experiments than predicted by models.

Investigation of a hydro-electric power machine was carried out by Feng and Chu[4] who predicted the orbits of a vertically configured pump/turbine with unevenly pre-loaded pads. Experimental work

[1]Division of Machine Elements, Luleå University of Technology, Luleå, Sweden
[2]LKAB, Kiruna, Sweden
[3]Machine Design, Royal Institute of Technology, Stockholm, Sweden
[4]Mechanics of Solid Materials, Luleå University of Technology, Luleå, Sweden
[5]Fluid and Experimental Mechanics, Luleå University of Technology, Luleå, Sweden
[6]Department of Mechanical Construction and Production, Ghent University, Ghent, Belgium

Corresponding author:
Gregory F Simmons, Division of Machine Elements, Luleå University of Technology, Lulea 97187, Sweden.
Email: gregory.simmons@lkab.com

with hydropower machines was conducted by Gustavsson et al.[5] and Nässelqvist[6] in which the authors determined the stiffness and damping of guide bearings experimentally using strain gages mounted on the structure and in the support pins of tilting pad bearings. These results were then compared to models for horizontal machines finding that the calculations for horizontal shaft eccentricity adequately predicted the vertical shaft's orbit magnitude. Aside from the work by Gustavsson, Nässelqvist and Aidanpää, very few experimental studies have focused on hydropower machines.

The limited number of experimental studies conducted on vertical rotating machines does not provide the accurate data needed to develop robust machine models to aid in development of new machines and upgrades and refurbishments of existing hydropower machines. Thus using the unique test facility at Porjus and a well-developed model, this study aims to begin filling in the gaps in experimental data and model studies regarding the guide bearings of large vertical rotating machines.

Equipment

The experimental work of this study was carried out on turbine-generator U9 at the old Porjus power station on the Lule River in the far north of Sweden. Turbine unit U9 (Figure 1) is unique in that its generator is directly connected to the electrical grid without transformers. The machine's Kaplan turbine has six runner blades, 20 guide vanes and 18 stay vanes and it operates at 600 rpm. Its three guide bearings are described in Table 1. While Porjus U9 is used occasionally in production, it is primarily used for research and development to improve and better understand hydropower facilities and their operation. To support the research goals, it is outfitted with an extensive sensor arrangement described in Cervantes et al.[7]

Relevant to the current work is that the housing of each of the machine's three guide bearings has four displacement sensors to measure shaft motion relative to the bearing. Four additional displacement sensors at each bearing are solidly mounted in the concrete foundation. Inside the bearing, each of the spherical pivot tilting pads has two displacement sensors to measure oil film thickness at the inlet and outlet of each pad and two type K thermocouples to measure oil temperature. Thermocouples are installed 6 mm below the pad surface using the technique developed in Glavatskih[8] which allows oil from the contact to continually leak past the thermocouple providing a faster response to oil film temperature changes. Furthermore, the pivot pin of each pad has been replaced with a load cell to directly measure pad load. The sensor arrangement for the pads is displayed in Figure 2.

Lubricant in the bearings for all testing was ISO VG68 turbine oil and is provided via a combination of oil bath and leading edge injection. The shaft rotates in the clockwise direction.

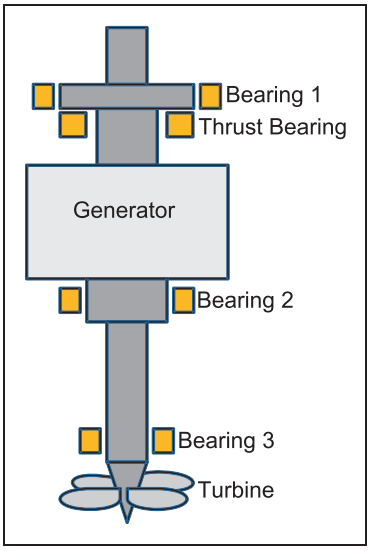

Figure 1. Arrangement of Porjus turbine/generator unit U9.

Table 1. Bearing characteristics.

Upper generator bearing (Bearing 1)	
Number of pads	6
Bearing diameter (mm)	956
Shaft diameter	955.57
Radial clearance (μm)	150
Pad length	28°
Pivot offset	64.3%
Pad height (mm)	150
Lower generator bearing (Bearing 2)	
Number of pads	6
Bearing diameter (mm)	651
Shaft diameter	650.57
Radial clearance (μm)	150
Pad length	35°
Pivot offset	61.4%
Pad height (mm)	150
Turbine bearing (Bearing 3)	
Number of pads	8
Bearing diameter (mm)	449.4
Shaft diameter	449.85
Radial clearance (μm)	150
Pad length	44°
Pivot offset	61%
Pad height (mm)	150

Uncertainty

The uncertainty associated with each of the measurements is presented in Table 2. Sources of uncertainty are primarily associated with the accuracy of the measurement equipment. In the case of film thickness

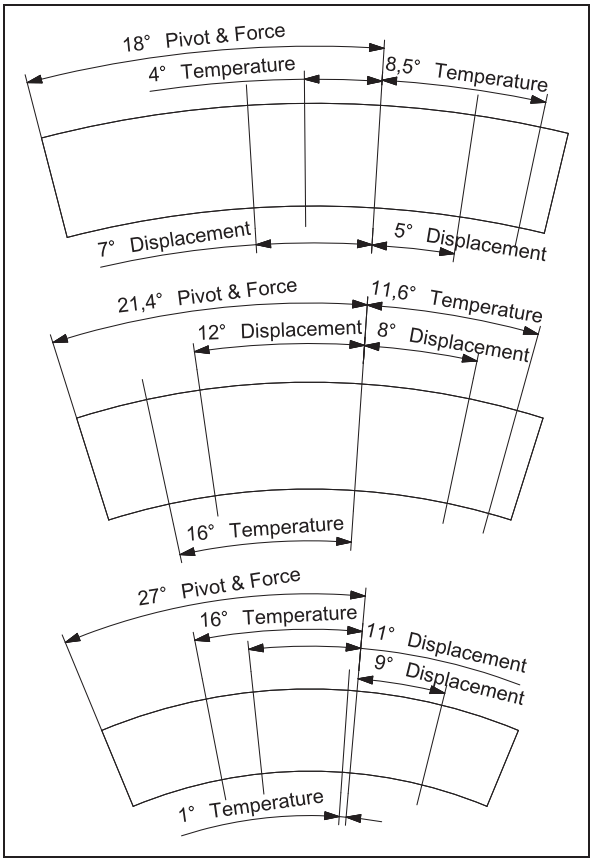

Figure 2. Sensor layout along the centerline for the pads of Bearing 1 (top), Bearing 2 (middle) and Bearing 3 (bottom). Sliding direction is from left to right.

Table 2. Measurement uncertainty.

Temperature	±1°C
Housing to shaft	±3 μm
Foundation to shaft	±4 μm
Film thickness	±2 μm

sensors, zero values for the sensors were found prior to installation but it was not possible to calibrate these values after assembly. Measurements of film thickness are therefore presented relative to the mean measurement from each sensor. Likewise, shaft orbit is determined from the center of the measured orbit. While the tolerances for roundness and form of the shaft in the bearing are small, the tolerances are not as small outside the bearing housing where the sensors used to determine shaft orbit are located. The error generated by these tolerances and roughness can be observed as a slight noise in the orbit plots and is included in the uncertainty of these measurements.

Model description

The multi-physics model used to simulate the bearing simultaneously solves the Reynolds equation, energy equation, equations of motion and pad deformation. The flow is assumed to be incompressible, viscous and laminar while the lubricant is considered to be Newtonian. All equations are solved using a commercial software package.[9] The time-dependent Reynolds equation as used in this model is written as follows

$$\frac{1}{R^2}\frac{\partial}{\partial\theta}\left(\frac{h^3}{\mu}\frac{\partial p}{\partial\theta}\right)+\frac{\partial}{\partial z}\left(\frac{h^3}{\mu}\frac{\partial p}{\partial z}\right)=6\Omega\frac{\partial h}{\partial\theta}+12\frac{\partial h}{\partial t} \quad (1)$$

The oil film thickness is given by the following expression

$$h = C_p-(C_p-C_b)\cos(\theta-\psi_i)$$
$$-(R+d)\partial_i\sin(\theta-\psi_i)+x\cos(\theta)+y\sin(\theta)+\partial_r \quad (2)$$

Equation (2) takes into account pad tilt in the circumferential (sliding) and axial directions. Radial displacement, ∂_r, term represents displacements due to both pad inclination and deflection. Mechanical and thermal deformations of the bearing are taken into account. Pressure at the pad edges is set to ambient. The pad-pivot interface is assumed to be a frictionless contact. The pivot is assumed to be rigid and with a 58 mm diameter. The density–pressure cavitation model is used to satisfy the flow continuity condition

$$\rho=\begin{cases}\rho_0 & \text{if } p>p_{sat}\\ \rho_0\left[3\left(\frac{p}{p_{sat}}\right)^2-2\left(\frac{p}{p_{sat}}\right)^3\right] & \text{if } p>p_{sat}\end{cases} \quad (3)$$

Saturation pressure is set to 20 kPa. The motion of the shaft mass center are given as follows

$$M\ddot{x}=F_x+M\xi\Omega^2\sin(\Omega t)$$
$$M\ddot{y}=F_y+M\xi\Omega^2\cos(\Omega t) \quad (4)$$

Deformation of the pad backing is calculated using a 6×6 elasticity matrix which takes into account stress and strain in the x, y and z directions.[9]

It has been demonstrated by a number of other researchers that temperature profile approximations across the film thickness in thermohydrodynamic analysis of journal bearings are more or less a good approximation technique compared to using the full energy equation.[10–13] Assuming that the heat conduction in the cross-film direction is much greater than the heat conduction in the circumferential and axial directions, the full energy equation can be simplified to the following by taking accounting for continuity equation

$$K\frac{\partial^2 T}{\partial y^2}-\rho c\left(u\frac{\partial T}{\partial\theta}+w\frac{\partial T}{\partial z}\right)$$
$$-\rho c\frac{\partial T}{\partial t}+\mu\left[\left(\frac{\partial u}{\partial y}\right)^2+\left(\frac{\partial w}{\partial y}\right)^2\right]=0 \quad (5)$$

where

$$u = \frac{1}{2\mu}\frac{\partial p}{\partial \theta}y^2 + \left(-\frac{h}{2\mu}\frac{\partial p}{\partial \theta} - \frac{U}{h}\right)y + U$$

$$w = \frac{1}{2\mu}\frac{\partial p}{\partial z}y^2\left(-\frac{h}{2\mu}\frac{\partial p}{\partial z}\right)y$$

where K, ρ and c are the thermal conductivity, density and specific heat of the lubricant, respectively. U is the rotating speed of the shaft, θ refers to the circumferential direction, z to the axial direction and y is the film thickness. In steady state conditions, such that $\partial T \partial t = 0$, and assuming that the shaft temperature is independent of the circumferential coordinate, $\partial T \partial \theta = \partial T_J \partial \theta = 0$ for $y = h$, evaluation of equation (5) on both the shaft and the bearing surface yields the following relations[10]

$$T''_B = \frac{\partial^2 T}{\partial y^2}||_{y-0} = -\frac{1}{K}\mu\left[\left(\frac{\partial u}{\partial y}\right)^2 + \left(\frac{\partial w}{\partial y}\right)^2\right]$$

$$T''_J = \frac{\partial^2 T}{\partial y^2}||_{y-h} = -\frac{1}{K}\mu\left[\left(\frac{\partial u}{\partial y}\right)^2 + \left(\frac{\partial w}{\partial y}\right)^2\right] \quad (6)$$

Because the derivatives T''_B and T''_J are independent of heat convection, equations (5) and (6) can be integrated by setting the following boundary conditions at the walls and the mid-plane of the film

$$T_B = T(0)$$
$$T_J = T(h)$$
$$T_m = \frac{1}{h}\int_0^h T(y)\mathrm{d}y \quad (7)$$

The temperature profile across the film is approximated by a fourth-order polynomial which allows determination of the analytical expression for the temperature profile

$$T(y) = ay^4 + by^3 + cy^2 + dy + e \quad (8)$$

where

$$a = \frac{1}{h^4}\left(5T_m - \frac{5}{2}(T_B + T_J) + \frac{5h^2}{24}(T''_B + T''_J)\right)$$
$$b = \frac{1}{h^3}\left(-10T_m + 5(T_B + T_J) - \frac{7h^2}{12}T''_B - \frac{h^2}{4}T''_J\right)$$
$$c = \frac{1}{2}T''_B$$
$$d = \frac{1}{h}\left(5T_m - \frac{7}{2}T_B - \frac{3}{2}T_J - \frac{h^2}{8}T''_B + \frac{h^2}{24}T''_J\right)$$
$$e = T_B \quad (9)$$

The heat exchange at the walls is determined as follows

$$q_B = K\frac{\partial T}{\partial y}||_{y-0} = K\left(5T_m - \frac{7}{2}T_B - \frac{3}{2}T_J - \frac{h^2}{8}T''_B + \frac{h^2}{24}T''_J\right)$$

$$q_J = K\frac{\partial T}{\partial y}||_{y-h} = K\left(5T_m - \frac{3}{2}T_B - \frac{7}{2}T_J - \frac{h^2}{24}T''_B + \frac{h^2}{8}T''_J\right) \quad (10)$$

Shaft temperature is calculated by integrating the heat exchange at the shaft surface and taking the average temperature. Thermal deformation of the bearing is calculated by

$$\Delta R = \alpha(T - T_0) \quad (11)$$

where α is the coefficient of thermal expansion for steel and T is the average bearing temperature. Furthermore, the viscosity–temperature relationship is used to predict the viscosity variation

$$\mu = \mu_0 \exp^{-\beta(T-T_0)} \quad (12)$$

A grid of $3 \times 26 \times 19$ nodes in the r, θ and z directions is used in the numerical model for each pad. A sensitivity study on the number of nodes in the compliant liner was performed and no visible difference was found. The final results are not affected by increasing the number of nodes in the pads. Since the pad is large, pad inertia must be taken into account. First, the static equilibrium position of the shaft is determined, and then the shaft is subjected to an unbalance force. The absolute convergence criteria for pressure and displacement are set to 10^{-7} Pa, 10^{-7} °C and 10^{-7} m. The convergence criteria of 10^{-9} was used to verify the accuracy of the final results and there was no visible difference between 10^{-7} and 10^{-9}. A time step of 50 μs is used.

Rotor dynamics modeling of the bearings was accomplished using a commercial rotor dynamics code.[14]

Results

Experimental results from the tests generally follow expectations from journal bearing theory. However, because most bearing models and practical experience are focused on horizontal machines, the presented experimental results have a number of important deviations from initial expectations.

Experimental results

The bearing temperatures measured in the guide bearings were highly dependent on the bearing's geometry but generally seem to be reasonable for hydrodynamic bearings[15] as shown in Tables 3 to 5. However, the

Table 3. Bearing and oil bath temperature in Bearing 1.

Location	Outlet, °C	Inlet, °C
Pad 1	58.3	50.8
Pad 2	58.0	50.7
Pad 3	60.9	51.0
Pad 4	56.8	49.3
Pad 5	56.2	49.7
Pad 6	58.6	51.3
Oil bath	32.6	25.3

pads of the most lightly loaded bearing, Bearing 3, appear to be significantly warmer than equally loaded pads in the other bearings. This extra heating is believed to be due to carryover of warm lubricant from one pad to the next which retains heat in the bearing and prevents cooling. Also of note is that the temperatures of several pairs of opposing pads (such as pad 3 and 6 in Bearing 2) are higher than the other pads. The temperatures in all of the pads correlate strongly with the load on each pad such that pads sitting opposite each other have similar temperatures.

Table 4. Bearing and oil bath temperature in Bearing 2 for experiment and maximum pad temperature from multi-physics model.

Location	Outlet, °C	Inlet, °C	Model, °C
Pad 1	54.0	40.1	47.0
Pad 2	51.4	39.3	47.2
Pad 3	59.8	48.9	47.0
Pad 4	48.8	36.6	47.0
Pad 5	54.1	40.2	47.2
Pad 6	57.4	42.0	47.0
Oil bath	38.2	28.4	40.0

Table 5. Bearing and oil bath temperature in Bearing 3.

Location	Outlet, °C	Inlet, °C
Pad 1	57.2	53.5
Pad 2	54.6	51.5
Pad 3	55.4	–
Pad 4	56.7	54.0
Pad 5	56.7	54.6
Pad 6	56.6	–
Pad 7	53.9	–
Pad 8	55.4	53.1
Oil bath	42.9	36.9

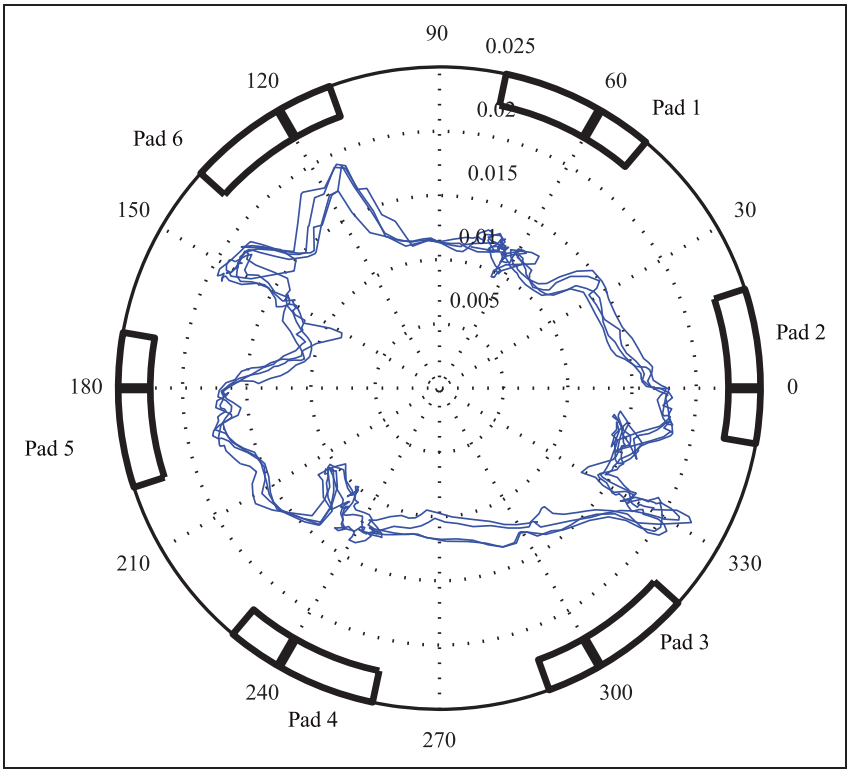

Figure 3. Orbit of the shaft in Bearing 1's housing. Dimensions are in mm and four complete orbits are shown.

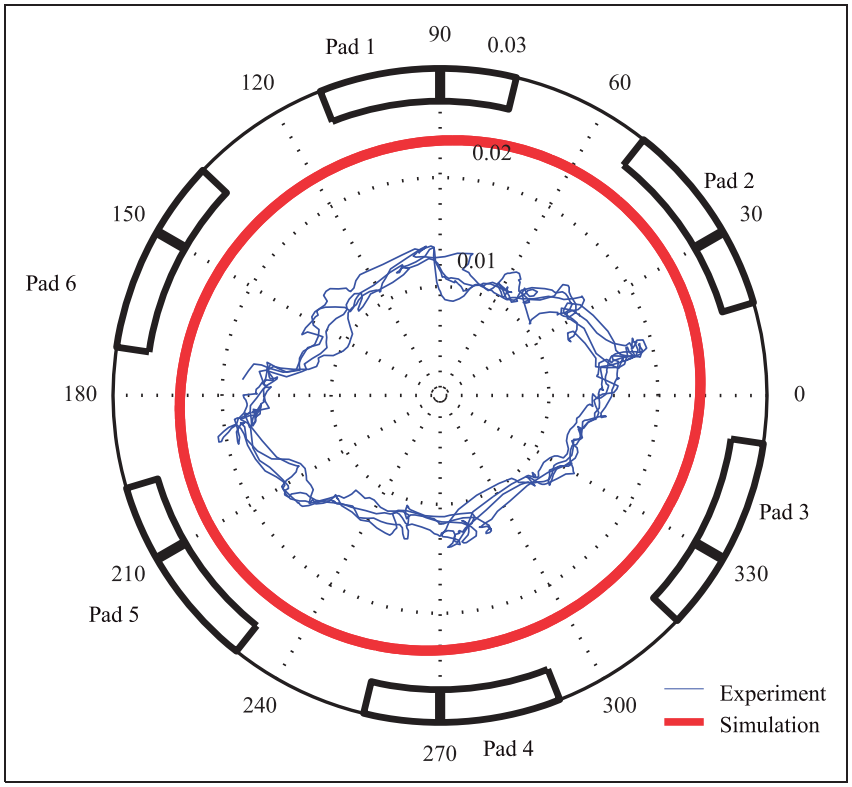

Figure 4. Orbit of the shaft in Bearing 2's housing from experiment and simulation. Dimensions are in mm and four complete orbits are shown. Pad locations are shown for reference.

Studies of the machine's bearings showed generally light loads and small orbits compared to loads in horizontal machines for electrical power generation. Shaft orbits within the upper bearings are provided in Figures 3 and 4. The load on each pad over the course of one revolution is shown in Figures 5 to 7 for Bearings 1, 2 and 3, respectively, which highlight the difference between journal bearings in vertical and horizontal machines. While the static load in a horizontal bearing is quite easily predicted, knowing the mass of the rotor and the bearing's geometry, the static load in a vertical bearing of a hydropower turbine is primarily affected by uneven pull by the generator, fluid effects in the turbine and the pre-load of the individual bearing pads. The effect of this can be observed in Figures 8 and 9 in which the bearing pad loads increase with rotation speed (Figure 10) and then shifts (at approximately 60 s) when the generator is connected to the electrical network. This leads to a maximum mean pressure on any individual bearing pad of approximately 0.4 MPa.

The evolution of the oil film temperature through the startup process is provided in Figure 11 for Bearing 1 and Figure 12 for Bearing 2. This temperature evolution further highlights the effects of the variation in pre-load of the individual bearing pads. In Bearing 1, the pads have a much smaller spread in temperatures than in Bearing 2 reflecting the more even pre-loading in Bearing 1 compared to Bearing 2.

The effect of the misalignment of the bearings correlates directly with the orbit of the shaft within the oil film. Taking into account the loads from Figure 6 and the orbit from the same instant shown in Figure 4, it can be observed that the most heavily loaded pads, Pad 6 and Pad 3, effectively force the orbit into an oval shape within Bearing 2.

While the static portion of the bearing load varied greatly for each set of opposing bearing pads, the dynamic portion of the pad load remained generally constant. A summation of the total dynamic load in Bearing 1 and Bearing 2 is provided in Figures 13 and 14, respectively. While some variation occurs through each revolution, the dynamic load appears to remain in the range of 2800 N in Bearing 1 and 1600 N in Bearing 2.

Bearing 2 had the greatest variation in film thickness and load between its pads. In Figure 6, it is observed that pads with the lightest load (pads 2 and 5) also had the greatest range of motion. Likewise, the most heavily loaded pads (pads 3 and 6) had the smallest range of motion. The pads of Bearing 3 are generally lightly loaded and the film thickness and tilt angle vary significantly over the course of one revolution as observed in Figure 7. Loads for pads 7 and 8 are not displayed as these two load cells were not operational.

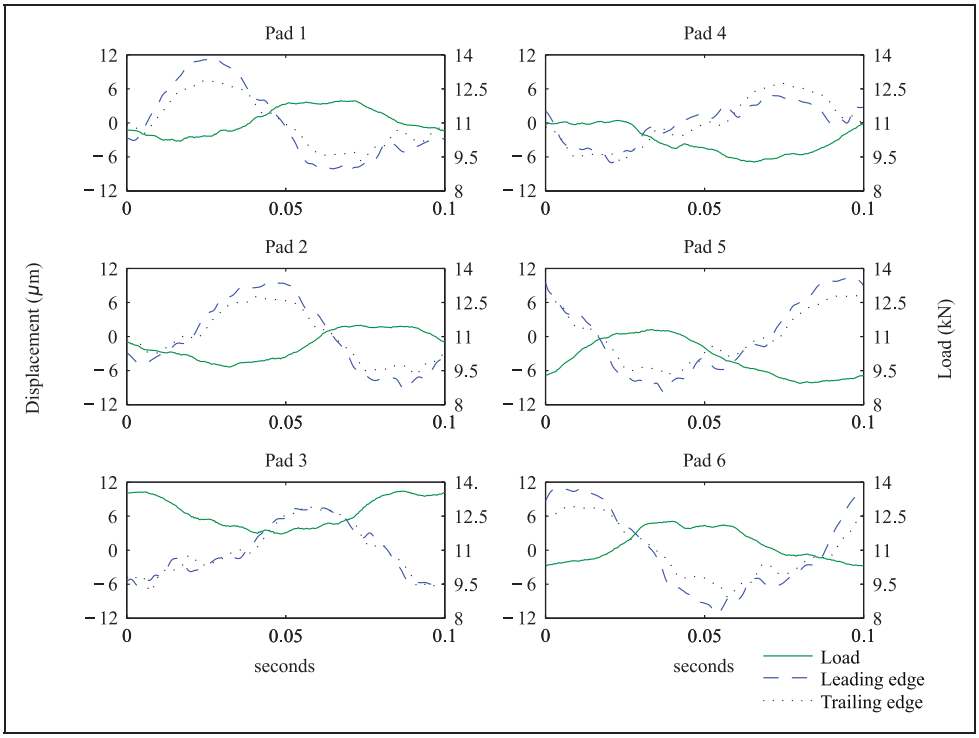

Figure 5. Bearing 1 dynamic portion of film thickness for the leading and trailing edges of all pads as well as the load on the pad over the course of one revolution.

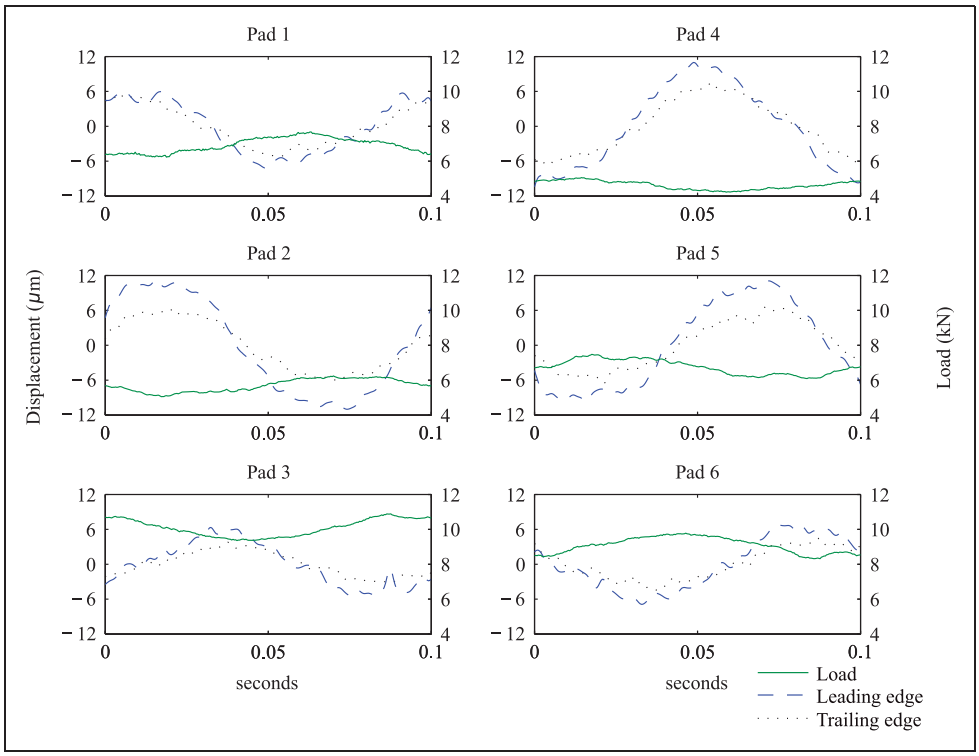

Figure 6. Bearing 2 dynamic portion of film thickness for the leading and trailing edges of all pads as well as the load on the pad over the course of one revolution.

Model results

The pre-load of each pad in the model was initially tuned to provide an identical orbit and static pad load to those observed in the experiments; however, when the orbit matched that of the experiments, the dynamic load on the individual pads was much lower than that observed. Matching the dynamic

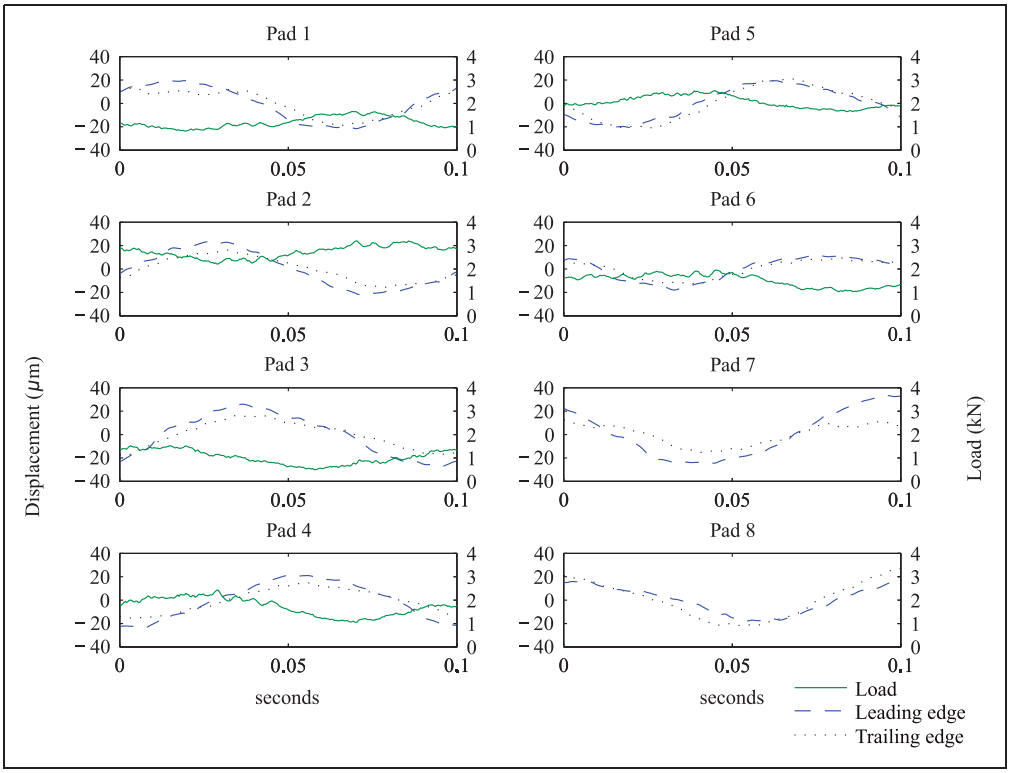

Figure 7. Bearing 3 dynamic portion of film thickness for the leading and trailing edges of all pads as well as the load on the pad over the course of one revolution.

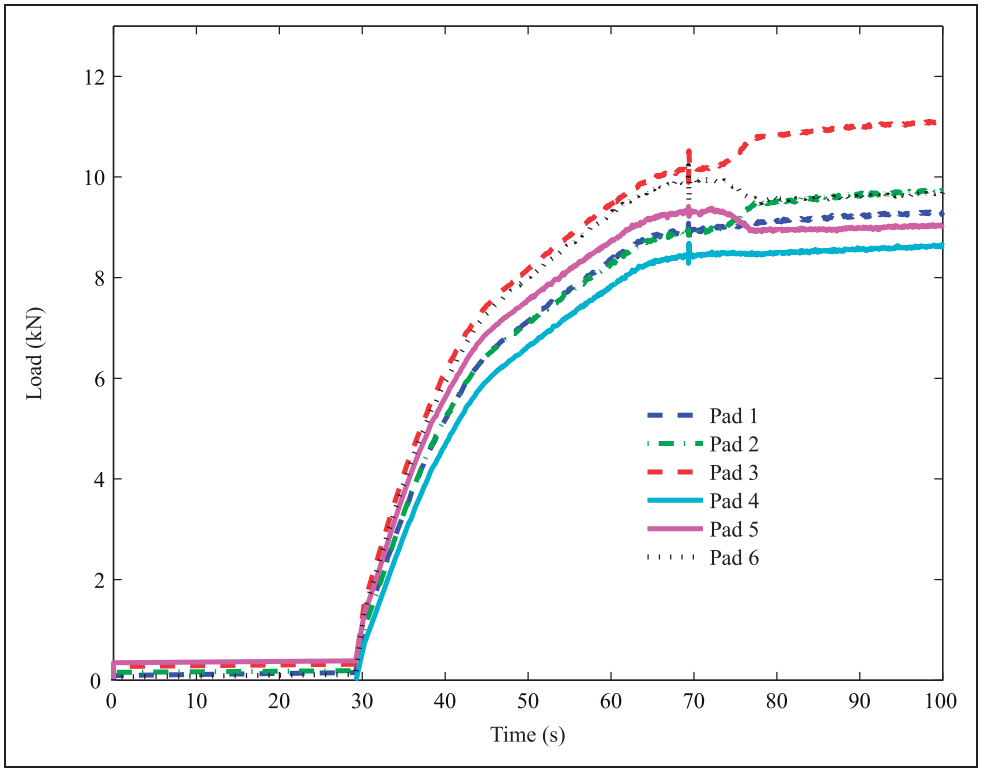

Figure 8. Static load on each pad during startup for Bearing 1. Rotor is connected to electrical grid at approximately 70 s.

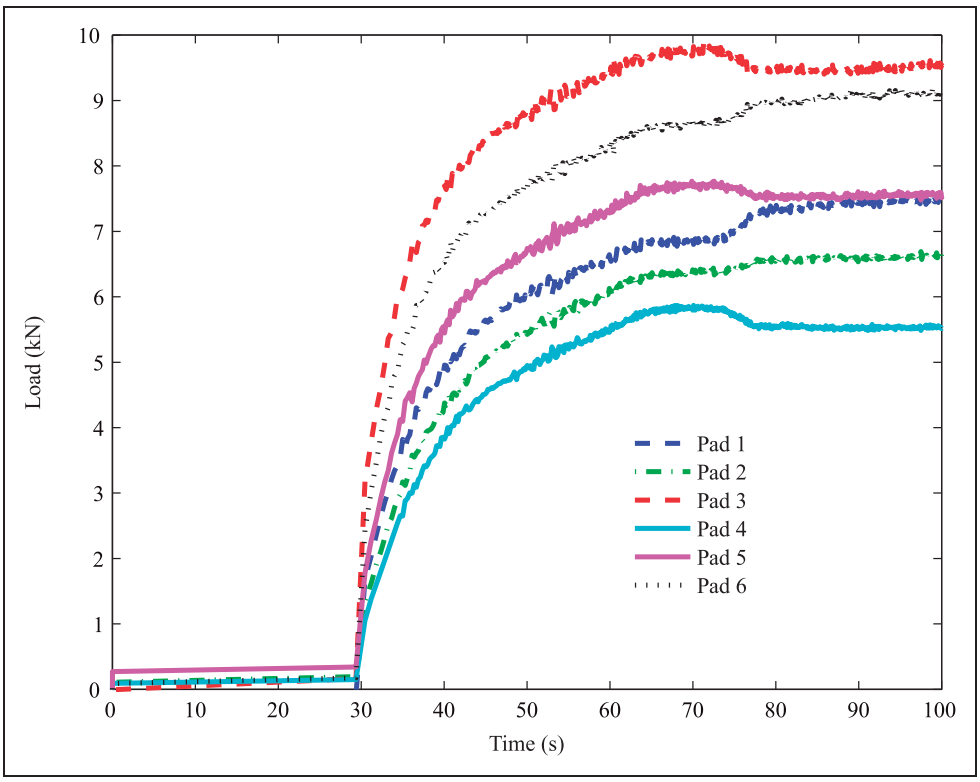

Figure 9. Static load on each pad during startup for Bearing 2. Rotor is connected to electrical grid at approximately 70 s.

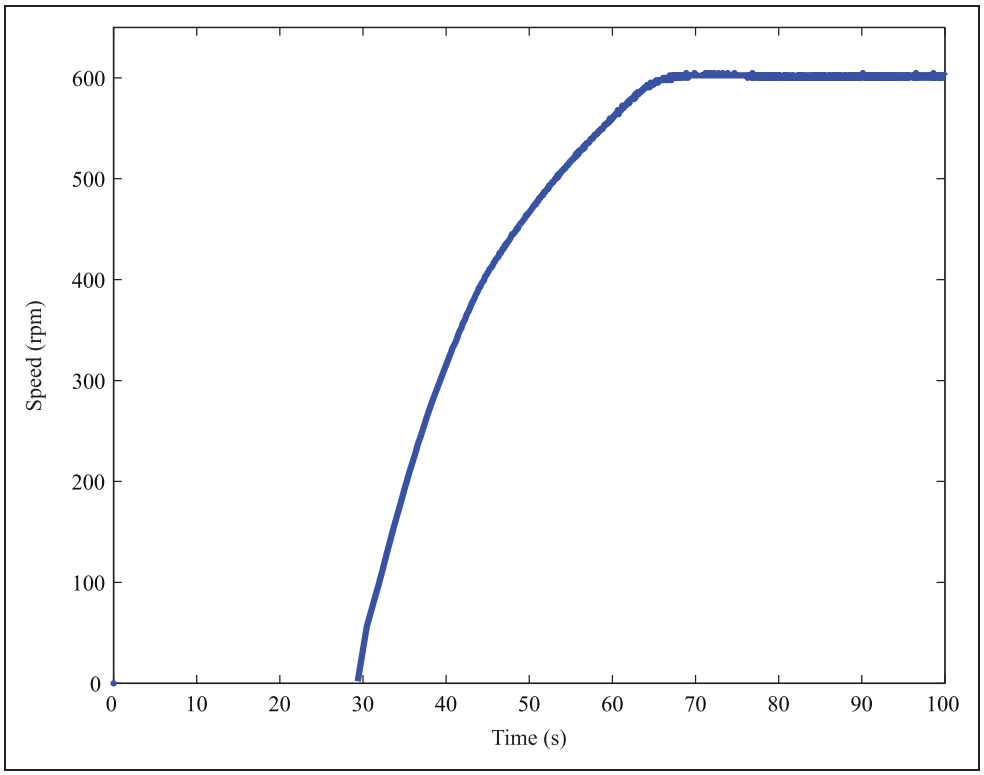

Figure 10. Machine speed during startup.

load and the static load led to the larger orbit shown in Figure 4. The discrepancy in orbit in this case is most likely due to the fact that the bearing's structure in the model is infinitely stiff. Calculation of the dynamic characteristics (Table 6) shows that this is not the case.

The pad temperatures in the model are lower due to a combination of factors. First, the model's method

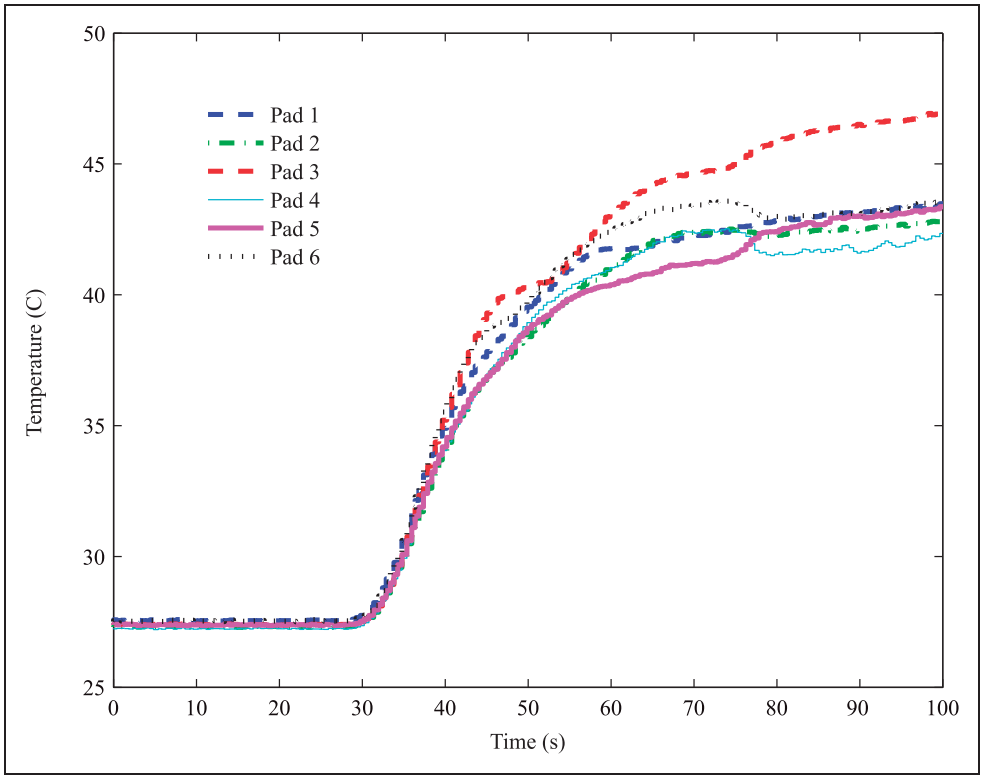

Figure 11. Temperature at the outlet side of each pad during startup for Bearing 1. Rotor is connected to electrical grid at approximately 70 s.

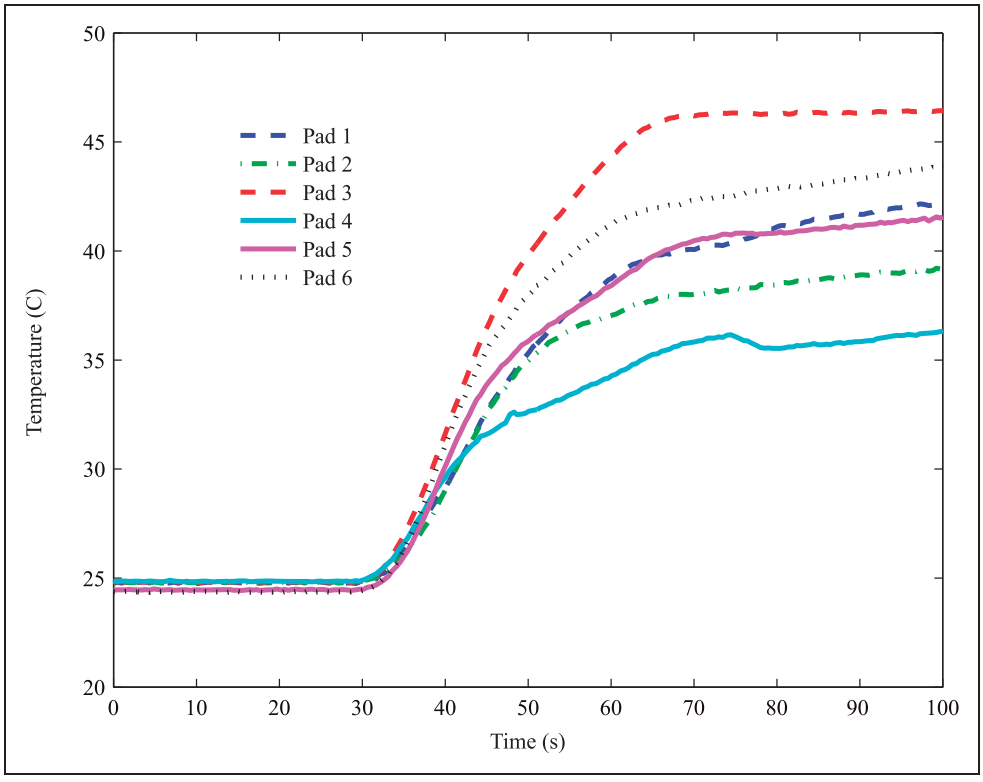

Figure 12. Temperature at the outlet side of each pad during startup for Bearing 2. Rotor is connected to electrical grid at approximately 70 s.

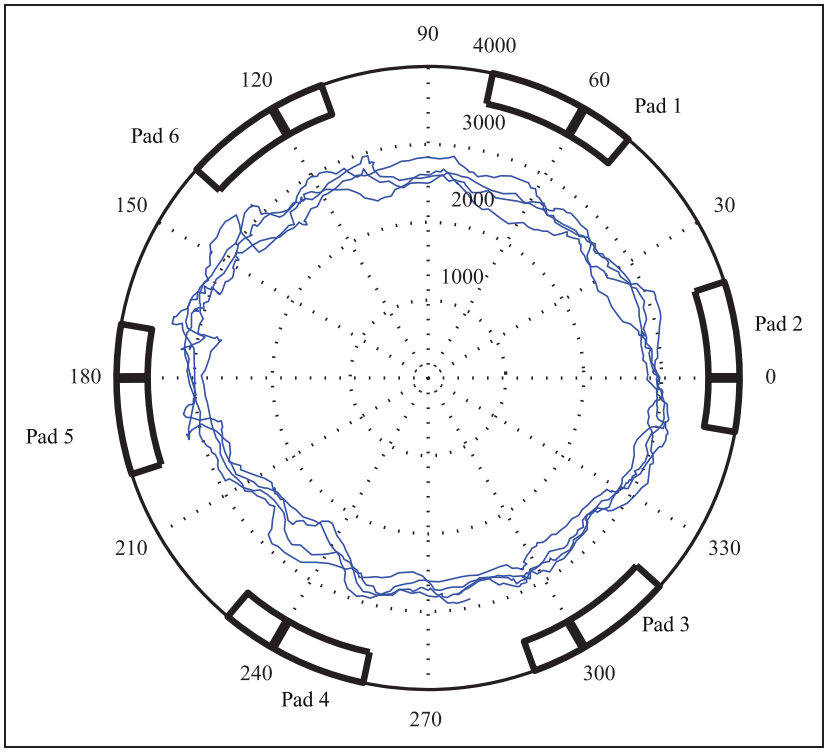

Figure 13. Dynamic portion of the bearing load in Bearing 1. Dimensions are in Newton and four complete orbits are shown.

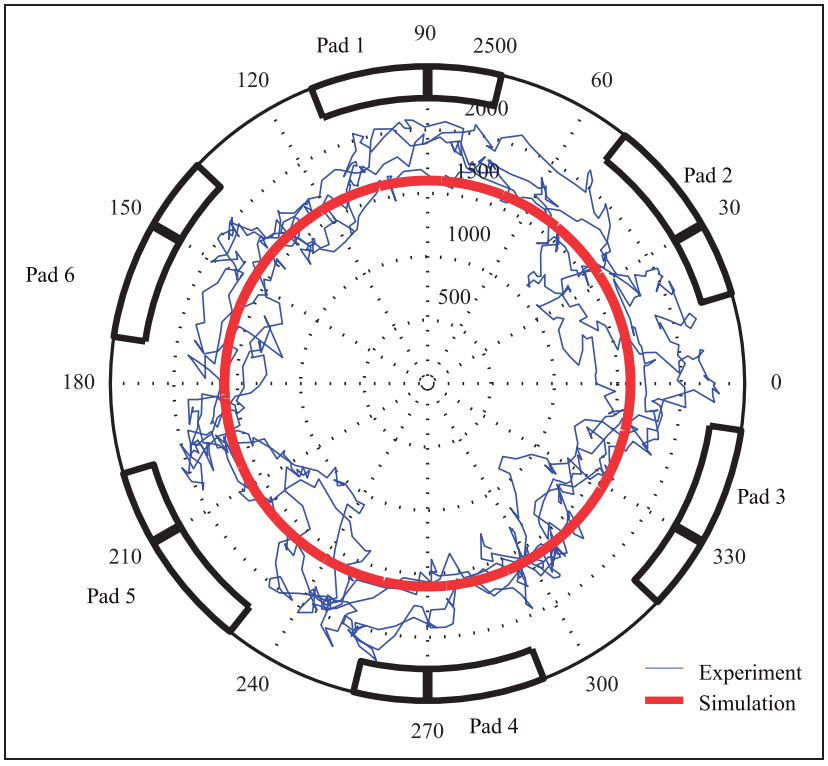

Figure 14. Dynamic portion of the bearing load in Bearing 2 from experiment and simulation. Dimensions are in Newton and four complete orbits are shown. Pad locations are shown for reference.

of handling the energy losses in the bearing is important to mention. To simplify the model and decrease computational time, a simplified energy equation is used which is not able to take into account all the energy used to shear the lubricant. The lower energy losses in turn lead to less heating of the lubricant and a thicker lubricant film for a given pad load. More importantly, the actual inlet temperature to the

bearing pads has large uncertainty. While the experiment gives a value for the oil at the surface of each pad, the oil at the shaft surface may be much warmer due to lubricant carryover from the previous pad.

Discussion

Experimental datasets gathered from full-scale machines are generally sparse in the academic literature. This is especially true for vertical hydropower turbines which until recent years have been almost entirely overlooked by the rotor dynamics and tribology research communities. From these initial results, it can be determined that while the machine generally behaves as would be expected from theory, the vertical configuration provides many unique effects. The inherent instability of the vertical rotor results in an orbit at a generally constant eccentricity as would be expected from a very lightly loaded horizontal machine. However, the light loading makes the bearing's performance more sensitive to unavoidable variation in assembly tolerances as described by Fillon, Dmochowski and Dadouche.[16,17] This sensitivity is very clear in the test results for the individual pads as exemplified by Bearing 2.

The experimental results allowed for calibration of the multi-physics model. As suggested by Feng and Chu,[4] by matching the orbit in the model with that measured in the experiment, it was possible to determine the degree of misalignment in the real bearing. In some cases, such as in Figure 4, the model was able to clarify the shaft motion with a more round orbit than that which was measured. It is believed that the squarish shape of the orbit in this case results from a combination of the construction of the machine with three bearings arranged on three different axes as well as possible slight misalignment of the displacement sensors. Such misalignments are unavoidable in large complex sensor installations when sensor installation must be adapted to real geometric and operational constraints.

The dynamic load and orbit in each of the bearings can be further used to characterize the stiffness and damping of the lubricant film, bearing and the foundation structure around the bearing using the methods of Gustavsson et al.[5] and Nässelqvist.[6] The mean stiffness of the three bearings calculated using this method is provided in Table 6 for the components of the bearings both immediately following startup (cold) and at steady state after several hours of operation (warm). Due to the complexity of the calculations, very large uncertainty (on the order of 20%) is associated with the stiffness values listed. This is especially important in Bearing 3 where data for two faulty load cells (on pads 7 and 8) was substituted with load measured from the opposing pads (pads 3 and 4) which was then shifted 180°. Housing stiffness is not calculated for Bearing 3 as the displacement sensors there provided unreliable data.

Table 6. Mean stiffness in the three bearings obtained from experiment (Exp) for both steady state (warm) and cold conditions, rotor dynamics model (RD), and multi-physics model (MP).

	Stiffness (N/m)	
Location	Warm	Cold
Bearing 1		
Oil film (Exp)	6.7×10^8	6.6×10^8
Oil film (RD)	6.3×10^8	–
Housing (Exp)	5.9×10^7	4.8×10^7
Foundation (Exp)	1.5×10^7	1.5×10^7
Bearing 2		
Oil film	5.3×10^8	6.3×10^8
Oil film (MP)	3.5×10^8	–
Oil film (RD)	4.2×10^8	–
Housing (Exp)	4.3×10^8	1.6×10^8
Foundation (Exp)	6.3×10^6	5.9×10^6
Bearing 3		
Oil film (Exp)	1.6×10^8	1.9×10^8
Oil film (RD)	3×10^8	–
Foundation (Exp)	1.1×10^7	1.2×10^7

The stiffness provided by each of the three bearings is closely related to the static load on the bearing pads. This is accentuated by Bearing 3 which has much lower stiffness than the other bearings due to the light static loading on its bearing pads.

Calculation of the stiffness from the multi-physics model results was accomplished using the same method as with the experimental results. The exception being that several rotations of the shaft were simulated by perturbing the model results with random noise. The multi-physics model predicts a lower stiffness than the experimentally determined value as is clear by the larger shaft orbit in the multi-physics model. A commercial rotor dynamics code (for horizontal machines) was also used to validate the calculations using the mean bearing pad load as the bearing load. All of these calculations are provided in Table 6.

From these stiffness calculations, it can be observed that the stiffness provided by the structure around the bearing is considerably lower than that of the oil film in the bearings. In order to allow for convergence in the rotor dynamics calculations and multi-physics model, this structural stiffness is assumed to be much higher than the oil film stiffness. The experimentally calculated stiffnesses demonstrate that this assumption is clearly incorrect and that the structure may be softer than the bearing oil film. This highlights that in design of hydropower plants, care should be taken to properly determine the characteristics of the structure surrounding the bearings to guarantee that the models used to develop the bearing and rotor design provide accurate results.

Furthermore, warming up of the machine seems to affect the different bearings differently. Bearing 1 and Bearing 2 become stiffer, but the oil film in Bearing 2 becomes softer after warm up. The stiffness of Bearing 3 on the other hand decreases slightly through the warm up process. Increasing the regularity of startup and shutdown increases the thermal cycling of the machine leading to constantly changing bearing characteristics. The long term effects of such a situation are uncertain but presumably could lead to less stability of the machine.

Conclusion

Experiments have been conducted in the journal bearings of a full-scale hydro-electric power machine to determine their characteristics. These experiments were then compared to a multi-physics model of one of the bearings and a rotor dynamics model including all bearings.

Variation in load, oil film thickness, pad tilting and temperature of the individual bearing pads was highly dependent on the alignment and individual pad preload from assembly.

A multi-physics model was able to capture many bearing characteristics, but the accuracy of the model was highly dependent on the boundary conditions including the accuracy of the bearing's geometry, the inherent misalignment that occurs at assembly and the response of the surrounding structure.

In hydropower machines, stiffness of the supporting structure may be more important to machine performance than the stiffness of the bearing alone and the stiffness can vary widely through a startup process due to the machine's thermal transients.

Funding

This research received no specific grant from any funding agency in the public, commercial, or not-for-profit sectors.

Conflict of interest

None declared.

Acknowledgments

The research presented in this paper was carried out as part of a project in conjunction with the Swedish Hydropower Center (SVC). SVC was established by the Swedish Energy Agency, Elforsk and Svenska Kraftnït in partnership with academic institutions. Additionally, the Porjus Stiftelsen is acknowledged for use of the experiment facilities in Porjus.

References

1. Dimond TW, Sheth PN and Allaire PE. Identification methods and test results for tilting pad and fixed geometry journal bearing dynamic coefficients – a review. *Shock Vib* 2009; 16: 13–43.
2. White MF, Torbergsen E and Lumpkin VA. Rotordynamic analysis of a vertical pump with tilting-pad journal bearings. *Wear* 1997; 207: 128–136.
3. San Andres L and De Santiago O. Identification of journal bearing force coefficients under high dynamic loading centered static operation. *Tribol Trans* 2005; 48: 9–17.
4. Feng F and Chu F. Influence of pre-load coefficient of TPJBS on shaft lateral vibration. *Tribol Int* 2002; 35: 65–71.
5. Gustavsson RK, Lundström ML and Aidanpää J-O. Determination of journal bearing stiffness and damping at hydropower generators using strain gauges. In: *Proceedings of PWR2005 ASME Power*, Chicago, IL, 2005, pp.5–7.
6. Nässelqvist M. *Simulation and characterization of rotordynamic properties for hydropower units*. Licentiate, Lulea University of Technology, 2009.
7. Cervantes MJ, Jansson I, Jourak A, et al. Porjus u9 a full-scale hydropower research facility. In: *24th symposium on hydraulic machinery and systems*, Foz do Iguassu, Brazil, 2008, pp.27–31.
8. Glavatskih SB. A method of temperature monitoring in fluid film bearings. *Tribol Int* 2004; 37: 143–148.
9. Comsol Multiphysics User's Guide, Version 3.5a, 2008.
10. Stefani A and Rebora F. Steadily loaded journal bearings: quasi-3d mass-energy-conserving analysis. *Tribol Int* 2009; 42: 448–460.
11. Sharma R and Pandey RK. An investigation into the validity of the temperature profile approximations across the film thickness in thd analysis of infinitely wide slider bearing. *Tribol Online* 2006; 1: 19–24.
12. Chauhan A, Sehgal R and Sharma R. Thermo-hydrodynamic analysis of elliptical journal bearing with different grade oils. *Tribol Int* 2010; 43: 1970–1977.
13. Chauhan A, Sehgal R and Sharma R. A study of thermal effects in an offset-halves journal bearing profile using different grade oils. *Lubricat Sci* 2011; 23: 233–248.
14. Rappid, Rotordynamics and Seal Research www.rsr.com.
15. Simmons GF and Glavatskih SB. Synthetic lubricants in hydrodynamic journal bearings: experimental results. *Tribol Lett* 2011; 42: 109–115.
16. Fillon M, Dmochowski W and Dadouche A. Numerical study of the sensitivity of tilting pad journal bearing performance characteristics to manufacturing tolerances: steady-state analysis. *Tribol Trans* 2007; 50: 387–400.
17. Dmochowski W, Dadouche A and Fillon M. Numerical study of the sensitivity of tilting-pad journal bearing performance characteristics to manufacturing tolerances: dynamic analysis. *Tribol Trans* 2008; 51: 573–580.